

A WENO algorithm for radiative transfer with resonant scattering: the time scale of the Wouthuysen-Field Coupling

Ishani Roy^a, Jing-Mei Qiu^b, Chi-Wang Shu^a, Li-Zhi Fang^c

^a*Division of Applied Mathematics, Brown University, Providence, RI 02912*

^b*Mathematical and Computer Science, Colorado School of Mines, Golden, CO 80401*

^c*Department of Physics, University of Arizona, Tucson, AZ 85721*

Abstract

We develop a numerical solver for the photon distribution in the frequency space described by radiative transfer with resonant scattering of Ly α photons by hydrogen gas in the early universe. This problem is crucial to the estimation of the time scale for the onset of the Wouthuysen-Field (WF) coupling in relation to the 21 cm emission and absorption at the epoch of reionization. The resonant scattering without recoil leads to the photon distribution in the frequency space to be piecewise smooth containing sharp changes. The weighted essentially nonoscillatory (WENO) scheme is suitable to handle this problem, as this algorithm has been found to be highly stable and robust for solving Boltzmann-like equations. We first show that the WENO solutions can precisely match the two analytic solutions of the evolution of the photon distribution in rest background. We find further that the evolution of the photon distribution due to resonant scattering without recoil generally undergoes three phases. First, the profile of the photon distribution is similar to the initial one. Second, an extremely flat plateau forms around the resonant frequency, and the width and height of the flat plateau increase with time. Finally, the distribution around the resonant frequency is stable (time-independent), as the photons from the source is balanced by the redshift of the expansion. This result indicates that the time-independent solutions of the Fokker-Planck approximation is questionable for describing the 21 cm problem, as the time scale of approaching the time-independent solution is of the order of one Myr, which might be longer than the evolutionary time scale of the 21 cm region around the first generation stars. However, the onset of the W-F coupling is not determined by the time-independent solution, but by the formation of the flat plateau of the second phase. We found that the time scale of the W-F coupling is only equal to about a few tens or hundreds of the mean free flight time of photons with resonant frequency, and it basically is independent of the Sobolev parameter if this parameter is much less than 1.

Key words: cosmology: theory, radiation, hydrodynamics, methods: numerical

PACS: 95.30.Jx, 07.05.Tp, 98.80.-k

1 Introduction

It is generally believed that detecting redshifted 21 centimeter signals from early universe is one of the next frontiers in observational cosmology, because it would be able to provide the information of the first generation of light sources in the cosmic dark ages. Many studies have been done on the 21 cm emission and absorption from the halo of individual first stars (Chuzhoy et al. 2006, Cen 2006, Liu et al. 2007). A common conclusion of these works is that the configurations of the 21 cm emission and absorption regions is strongly time-dependent. The reason is simple. The necessary conditions of 21 cm emission and absorption are that 1. the fraction of neutral hydrogen (HI) is still high; 2, Ly α photons are available for the Wouthuysen-Field (W-F) coupling. Therefore, the region of 21 cm emission and absorption around first stars has to be the shell just outside the I-front (ionization-front). Hence the 21 cm emission and absorption shell should move with a speed higher than the speed of the I-front v_f , which is rather high, even comparable to the speed of light. Therefore, the time scale of the formation and evolution of the regions of 21 cm signal can be estimated by d/v_f , d being the thickness of the 21 cm emission and absorption shell. This time scale is found to be of the order of 1 Myr or even less (Cen 2006, Liu et al. 2007).

In all of the above-mentioned works, the spin temperature is calculated with the assumption that the Wouthuysen-Field (W-F) coupling (Wouthuysen, 1952; Field, 1958, 1959) is effective. That is, the color temperature of photons around Ly α frequency is assumed to be the same as the kinetic temperature of hydrogen gas. The W-F coupling locks the color temperature of Ly α photon to the kinetic temperature of hydrogen gas, and then links the internal (spin-) degree of freedom with the kinetic temperature of gas. Obviously, the application of the W-F coupling would be reasonable if the time scale of the onset of the W-F coupling is less than the time scale of the formation and evolution of the 21 cm emission and absorption shells. However, most calculations on the W-F coupling are based on the *time-independent* Fokker-Planck approximation (Chen & Miralda-Escude, 2004; Hirata, 2006; Furlanetto & Pritchard 2006; Chuzhoy & Shapiro 2006). The time-independent solution would be acceptable if the time-independent state is approached in a time scale shorter than that of the evolution of the 21 cm signal regions. Unfortunately, we find that this assumption is not always correct. Therefore, a time-dependent solution is necessary.

The W-F coupling is due to the resonant scattering of Ly α photons by hydrogen atoms. It is described by a Boltzmann-like integro-differential equation of radiative distribution in the phase space. The W-F coupling is sensitive to the evolution of the photon distribution in the frequency space. The frequency distribution of photons under the kinetics of resonant scattering of Ly α photons by gaseous hydrogen atoms without recoil shows two features: 1. an extremely flat top of the photon profiles in the frequency space; 2. a sharp boundary of the flat top range. These features can be seen from the two analytical solutions of the evolution of the photon distribution in rest background (Field 1958). Currently, the numerical results are still far from precise to match these features (e.g. Meiksin, 2006).

In this paper, we develop a numerical solver with the weighted essentially nonoscillatory (WENO) scheme. The WENO method has high order of accuracy and good convergence in capturing discontinuities as well as to be significantly superior over piecewise smooth solutions containing discontinuities (Shu 2003). WENO schemes have been widely used in applications. It is also effective to solve Boltzmann equations (Carrillo et al. 2003, 2006) and radiative transfer (Qiu et al. 2006, 2007, 2008). Therefore, one can expect that the two features (flat top and sharp boundary) can also be properly handled numerically by the WENO scheme.

The paper is organized as follows. Section 2 presents the basic equations of the resonant scattering of radiation. Section 3 gives the numerical solver of the WENO scheme. Section 4 is to test the numerical solver with Field's analytic solutions. Section 5 shows the numerical solutions of the resonant scattering of photons. The time scale of the W-F coupling is addressed in Section 6. A discussion and conclusion are given in Section 7.

2 Basic equations

2.1 Radiative transfer equations with resonant scattering

Considering a spatially homogeneous and isotropically expanding infinite medium consisting of neutral hydrogen with temperature T , the kinetics of photons in the frequency space is described by the radiative transfer equation with resonant scattering (Hummer & Rybicki, 1992; Rybicki & Dell'antonio 1994)

$$\begin{aligned} \frac{\partial J(x, t)}{\partial t} + 2HJ(x, t) - \frac{cH}{v_T} \frac{\partial J(x, t)}{\partial x} = \\ -kc\phi(x)J(x, t) + kc \int \mathcal{R}(x, x')J(x', t)dx' + C(t)\phi(x) \end{aligned} \quad (1)$$

where J is the specific intensity in terms of the photon number, $H(t) = \dot{a}(t)/a(t)$ is the Hubble parameter, a is the cosmic factor, $v_T = (2k_B T/m)^{1/2}$ is the thermal velocity of hydrogen atom, the dimensionless frequency x is related to the frequency ν and the resonant frequency ν_0 by $x = (\nu - \nu_0)/\Delta\nu_D$, and $\Delta\nu_D = \nu_0 v_T/c$ is the Doppler broadening. The parameter $k = \chi/\Delta\nu_D$, and the intensity of the resonant absorption χ is given by $\chi = \pi e^2 n_1 f_{12}/m_e c$, where n_1 the number density of neutral hydrogen HI at ground state, and $f_{12} = 0.416$ is the oscillation strength. The cross section at the line center is

$$\sigma_0 = \frac{\pi e^2}{m_e c} f_{12} (\Delta\nu_D)^{-1}. \quad (2)$$

In eq.(1), $C(t)$ is the source of photons with the frequency distribution $\phi(x)$, which is the Voigt function of the frequency profile with the center at ν_0 , i.e.

$$\phi(x) = \frac{a}{\pi^{3/2}} \int_{-\infty}^{\infty} dy \frac{e^{-y^2}}{(x-y)^2 + a^2} \quad (3)$$

where a is the ratio of the natural to the Doppler broadening. We have $a = A_{21}/(8\pi\Delta\nu_D)$, and $A_{21} = 6.25 \times 10^8$ Hz is the Einstein spontaneous emission coefficient. $\phi(x)$ is normalized with $\int \phi(x') dx' = 1$. When $a \rightarrow 0$, we have pure Doppler broadening as

$$\phi_D(x) = \frac{1}{\sqrt{\pi}} e^{-x^2}. \quad (4)$$

The redistribution function $\mathcal{R}(x, x')$ gives the probability of a photon absorbed at the frequency x , and re-emitted at the frequency x' . It depends on the details of the scattering (Henyey 1941; Hummer 1962; Hummer, 1969). If we consider coherent scattering without recoil, it is

$$\mathcal{R}(x, x') = \frac{1}{\pi^{3/2}} \int_{|x-x'|/2}^{\infty} e^{-u^2} \left[\tan^{-1} \left(\frac{x_{\min} + u}{a} \right) - \tan^{-1} \left(\frac{x_{\max} - u}{a} \right) \right] du \quad (5)$$

where $x_{\min} = \min(x, x')$ and $x_{\max} = \max(x, x')$. Obviously, $\int_{-\infty}^{\infty} \mathcal{R}(x, x') dx' = \phi(x)$. In the case of $a = 0$, i.e. considering only the Doppler broadening, eq.(5) becomes

$$\mathcal{R}(x, x') = \frac{1}{2} \operatorname{erfc}[\max(|x|, |x'|)]. \quad (6)$$

2.2 Re-scaling the equations

We use the new time variable τ defined as $\tau = cn_1\sigma_0 t$, which is in units of the mean free flight time of photons at resonant frequency. The number density of neutral hydrogen atoms $n_1 = f_{\text{HI}}n_{\text{H}}$, with f_{HI} being the fraction of neutral hydrogen. For the concordance Λ CDM model, we have $n_{\text{H}} = 0.75 \times 1.88 \times 10^{-7}(\Omega_b h^2/0.02)(1+z)^3 \text{ cm}^{-3}$. The factor 0.75 is from hydrogen abundance. Therefore,

$$t = 0.071\tau f_{\text{HI}}^{-1} \left(\frac{T}{10^4}\right)^{1/2} \left(\frac{10}{1+z}\right)^3 \left(\frac{0.02}{\Omega_b h^2}\right) \text{ yrs} \quad (7)$$

We re-scale the eq.(1) by the following new variables

$$J'(x, t) = [a(t)/a_0]^2 J, \quad C'(t) = [a(t)/a_0]^2 C. \quad (8)$$

Thus, eq.(1) becomes

$$\begin{aligned} \frac{\partial J'(x, \tau)}{\partial \tau} &= -\phi(x)J'(x, \tau) \\ &+ \int \mathcal{R}(x, x')J'(x', \tau)dx' + \gamma \frac{\partial J'}{\partial x} + C'(\tau)\phi(x). \end{aligned} \quad (9)$$

We will use J for J' and C for C' in the equations below. The parameter γ is the so-called Sobolev parameter, $\gamma = (H/v_T k) = (8\pi H/3A_{12}\lambda^3 n_1) = (Hm_e\nu_0/\pi e^2 n_1 f_{12})$, where λ is the wavelength for Ly α transition. γ is simply related to the Gunn-Peterson optical depth τ_{GP} by

$$\gamma^{-1} = \tau_{GP} = 3.7 \times 10^5 h^{-1} f_{\text{HI}} \left(\frac{0.25}{\Omega_M}\right)^{1/2} \left(\frac{\Omega_b h^2}{0.02}\right) \left(\frac{1+z}{10}\right)^{3/2}. \quad (10)$$

The redshift evolution of f_{HI} is dependent on the reionization models. Before reionization $f_{\text{HI}} \simeq 1$; after reionization $f_{\text{HI}} \simeq 10^{-5}$ in average. Therefore, the parameter γ has to be in the range from 1 ($z \leq 7$) to 10^{-7} ($z \geq 10$). For static background, $\gamma = 0$.

In the Fokker-Planck approximation, eq.(9) becomes (Hummer & Rybicki, 1992; Rybicki & Dell'antonio 1994)

$$\frac{\partial J(x, \tau)}{\partial \tau} = \frac{1}{2} \frac{\partial}{\partial x} \left[\phi(x) \frac{\partial J(x, \tau)}{\partial x} \right] + \gamma \frac{\partial J}{\partial x} + C(\tau)\phi(x). \quad (11)$$

The first term on the R.H.S. of eq.(11) describes the diffusion in the frequency space due to the resonant scattering.

3 Numerical solver: the WENO scheme

3.1 Computational domain and computational mesh

The computational domain in the case of static background is $x \in [-6, 6]$. The initial condition is $J(x, 0) = 0$. The boundary condition is

$$J(x, \tau) = 0, \quad \text{at } |x| = 6. \quad (12)$$

In the case of expanding background, i.e. $\gamma \neq 0$, the computational domain is bigger than $x \in [-6, 6]$ depending on the value of the Sobolev parameter γ . The domain (x_{left}, x_{right}) is chosen such that for the particular value of γ we have

$$J(x_{left}, \tau) \approx 0, \quad J(x_{right}, \tau) \approx 0. \quad (13)$$

For example, the domain is taken to be $x \in [-100, 6]$ for the case of $\gamma = 10^{-3}$. Also for different values of γ the solutions reach saturation at different time. For example, we see in our numerical results that the solution $J(\nu, t)$ of eq. (9) reaches saturation at time $\tau = 100$ for $\gamma = 10^{-1}$, and reaches saturation at time $\tau = 10^4$ for $\gamma = 10^{-3}$. The computational domain is discretized into a uniform mesh in the x direction,

$$x_i = x_{left} + i\Delta x, \quad i = 0, 1, 2, \dots, N_x,$$

where $\Delta x = (x_{right} - x_{left})/N_x$, is the mesh size. We also denote $J_i^n = J(x_i, \tau^n)$, the approximate solution values at (x_i, τ^n) .

3.2 Algorithm of the spatial derivative

To calculate $\frac{\partial J}{\partial x}$, we use the fifth order WENO method (Jiang & Shu, 1996). That is,

$$\frac{\partial J(x_i, \tau^n)}{\partial x} \approx \frac{1}{\Delta x}(\hat{h}_{j+1/2} - \hat{h}_{j-1/2}) \quad (14)$$

where the numerical flux $\hat{h}_{j+1/2}$ is obtained by the procedure given below. We use the upwind flux in the fifth order WENO approximation because the wind direction is fixed (negative). First we denote

$$h_i = J(x_i, \tau^n), \quad i = -2, -1, \dots, N_x + 3 \quad (15)$$

where n is fixed. The numerical flux from the WENO procedure is obtained by

$$\hat{h}_{i+1/2} = \omega_1 \hat{h}_{i+1/2}^{(1)} + \omega_2 \hat{h}_{i+1/2}^{(2)} + \omega_3 \hat{h}_{i+1/2}^{(3)}, \quad (16)$$

where $\hat{h}_{i+1/2}^{(m)}$ are the three third order fluxes on three different stencils given by

$$\begin{aligned} \hat{h}_{i+1/2}^{(1)} &= -\frac{1}{6}h_{i-1} + \frac{5}{6}h_i + \frac{1}{3}h_{i+1}, \\ \hat{h}_{i+1/2}^{(2)} &= \frac{1}{3}h_i + \frac{5}{6}h_{i+1} - \frac{1}{6}h_{i+2}, \\ \hat{h}_{i+1/2}^{(3)} &= \frac{11}{6}h_{i+1} - \frac{7}{6}h_{i+2} + \frac{1}{3}h_{i+3}, \end{aligned}$$

and the nonlinear weights ω_m are given by,

$$\omega_m = \frac{\check{\omega}_m}{\sum_{l=1}^3 \check{\omega}_l}, \quad \check{\omega}_l = \frac{\gamma_l}{(\epsilon + \beta_l)^2}, \quad (17)$$

where ϵ is a parameter to avoid the denominator to become zero and is taken as $\epsilon = 10^{-8}$. The linear weights γ_l are given by

$$\gamma_1 = \frac{3}{10}, \quad \gamma_2 = \frac{3}{5}, \quad \gamma_3 = \frac{1}{10}, \quad (18)$$

and the smoothness indicators β_l are given by

$$\begin{aligned} \beta_1 &= \frac{13}{12}(h_{i-1} - 2h_i + h_{i+1})^2 + \frac{1}{4}(h_{i-1} - 4h_i + 3h_{i+1})^2, \\ \beta_2 &= \frac{13}{12}(h_i - 2h_{i+1} + h_{i+2})^2 + \frac{1}{4}(h_i - h_{i+2})^2, \\ \beta_3 &= \frac{13}{12}(h_{i+1} - 2h_{i+2} + h_{i+3})^2 + \frac{1}{4}(3h_{i+1} - 4h_{i+2} + h_{i+3})^2. \end{aligned}$$

3.3 High order numerical integration

The integration of the resonance scattering term is calculated by a fifth order quadrature formula (Shen et al. 2007)

$$\int_{x_{left}}^{x_{right}} f(x)dx = \Delta x \sum_{j=0}^{N_x} w_j f(x_j) + O(\Delta x^5), \quad (19)$$

where the weights are defined as,

$$w_0 = \frac{251}{720}, \quad w_1 = \frac{299}{240}, \quad w_2 = \frac{211}{240}, \quad w_3 = \frac{739}{720},$$

$$w_{N_x-3} = \frac{739}{720}, \quad w_{N_x-2} = \frac{211}{240}, \quad w_{N_x-1} = \frac{299}{240}, \quad w_{N_x} = \frac{251}{720},$$

and $w_j = 1$ otherwise. Notice that this numerical integration is very costly and uses most part of the CPU time. For the case with $a = 0$, we have used a grouping of the numerical integration operations at different x locations so that the computational cost can be reduced to order $O(N)$ rather than $O(N^2)$, where N is the number of grid points in x , without changing mathematically the algorithm and its accuracy. Unfortunately, this grouping technique does not work for the case $a \neq 0$, hence the CPU cost for the case with $a \neq 0$ is much larger.

3.4 Time evolution

To evolve in time, we use the third-order TVD Runge-Kutta time discretization (Shu & Osher, 1988). For systems of ODEs $u_t = L(u)$, the third order Runge-Kutta method is

$$u^{(1)} = u^n + \Delta\tau L(u^n, \tau^n),$$

$$u^{(2)} = \frac{3}{4}u^n + \frac{1}{4}(u^{(1)} + \Delta\tau L(u^{(1)}, \tau^n + \Delta\tau)),$$

$$u^{(3)} = \frac{1}{3}u^n + \frac{2}{3}(u^{(2)} + \Delta\tau L(u^{(2)}, \tau^n + \frac{1}{2}\Delta\tau)).$$

4 Tests with analytical solutions of static background

We first test the WENO solver with two analytical solutions of eq. (9) (Field, 1958). For static background, $H = \gamma = 0$, Doppler broadening $a = 0$, if the initial radiative field is zero, $J(x, \tau) = 0$ and the constant source $C(\tau) = 1$, an analytical solution of eq.(9) is

$$J(x, \tau) = \pi^{-1/2}[1 - \exp(-\tau e^{-x^2})] + \int_x^\infty e^{w^2} [1 - (1 + \tau e^{-w^2}) \exp(-\tau e^{-w^2})] \text{erf}(w) dw. \quad (20)$$

The second analytical solution of eq.(9) is also for $H = \gamma = 0$, $a = 0$, but the source $C = 0$, while the initial radiative field is

$$J(\nu, 0) = \pi^{-1/2} e^{-\nu^2}. \quad (21)$$

The solution is

$$J(x, \tau) = \pi^{-1/2} e^{-x^2} \exp(-\tau e^{-x^2}) + \tau \int_x^\infty e^{-w^2} \exp(-\tau e^{-w^2}) \text{erf}(w) dw. \quad (22)$$

The analytical solutions (20) and (22) are shown in Figures 1 and 2 respectively. We also plot the numerical solutions in those figures. The numerical results show very small deviation from the analytical solutions. Therefore, the numerical integration and time evolution algorithm are reliable.

A common feature of Figures 1 and 2 is that the originally Doppler peak at the center of the frequency profile gradually becomes a flat plateau. The width of the plateau increases with time. This is because the resonant scattering makes a non-uniform distribution in the frequency space to a uniform one. It is similar to that in the physical space, diffusion generally leads to an evolution from non-uniform distribution to a uniform one. The height of the plateau of Figure 1 is increasing with time, while in Figure 2 it is decreasing, because for the case $C = 1$, the number of photons increases, while for the case of $C = 0$, the total number of photons is conserved.

As we know, the Fokker-Planck approximation eq.(11) would be proper if $J(x, \tau)$ is a slowly varying function of x , but poor if it is a strong x -function. Therefore, the solution with the Fokker-Planck approximation has large errors with the sharp boundary of the flat plateau. It shows significant deviation from the analytical solution eqs.(20) and (22) (e.g. Meiksin 2006).

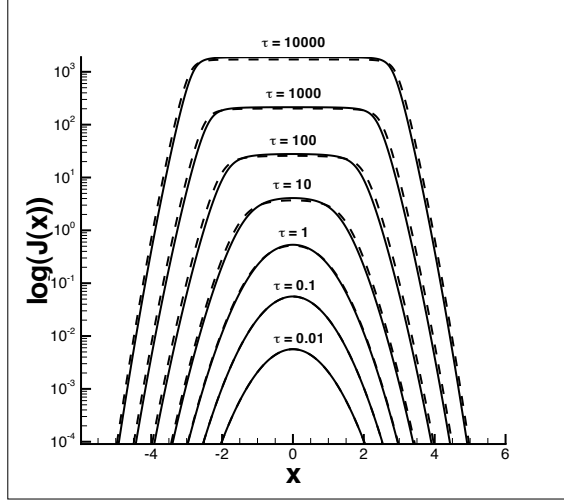


Fig. 1. Static solutions ($\gamma = 0$) for pure Doppler redistribution ($a = 0$) of eq.(9), in which $C = 1$ and $J(x, 0) = 0$. The analytical solutions are shown by dashed lines, while the numerical results are shown by solid lines.

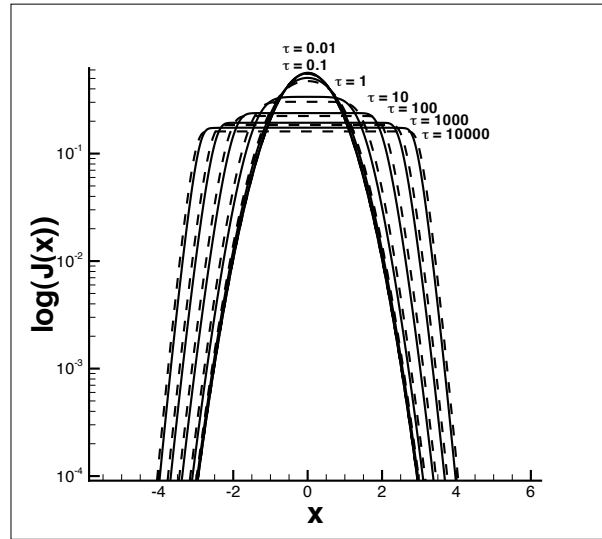


Fig. 2. Static solutions ($\gamma = 0$) for pure Doppler redistribution ($a = 0$) of eq.(9), in which $C = 0$ and $J(x, 0) = \pi^{-1/2} \exp(-x^2)$. The analytical solutions are shown by dashed line, while the numerical results are shown by solid lines.

5 Solutions with expanding background

Now we solve the eq.(9) with $\gamma \neq 0$, i.e. the background is expanding. In this case, the frequency of photons will be redshifted. Eq.(9) has two parameters γ and a . We first consider the Doppler broadening, $a = 0$. The initial radiative field is assumed to be zero $J(x, 0) = 0$, and a uniformly Ly α photon source in the physical space is taking place at $\tau = 0$. Since eq.(9) is linear, the solutions with different intensity C are linearly related. We take $C(\tau) = 1$.

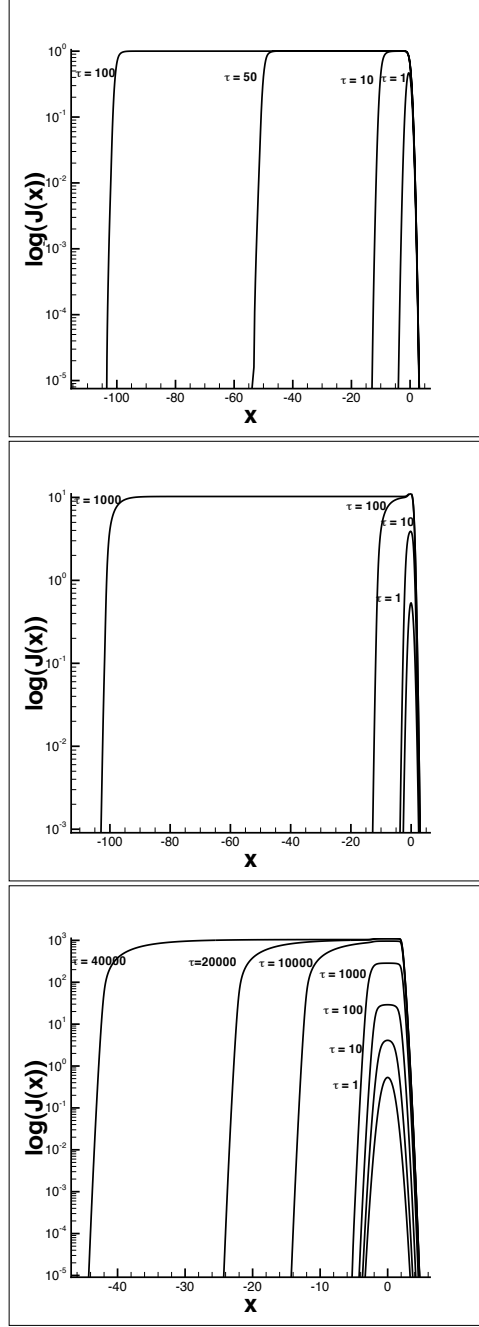


Fig. 3. Solutions of $J(x, t)$ of eq.(9). The parameters $a = 0$ and $\gamma = 1$ (top), $\gamma = 10^{-1}$ (middle) and $\gamma = 10^{-3}$ (bottom).

Figure 3 presents the solutions $J(x, \tau)$ for $\gamma = 1, 10^{-1}$ and 10^{-3} . The evolutions of $J(x, \tau)$ for these three cases are similar. Roughly, it can be divided into three phases. When τ is small, $J(x, \tau)$ keeps the initial Gaussian profile $\phi(x)$ of the photons from source C . This is the first phase. In the second phase, the profile is no longer Gaussian. A flat plateau forms on the top due to the resonant scattering. The width of the flat plateau increases with the time τ . This is like the cases shown in Figures 1 and 2. Finally, when the injection of Ly α

photons from the source C is balanced by the redshift, the height of the flat plateau of $J(x, \tau)$ will stop increasing. The width of the flat plateau on the red side continuously increases. This is the third phase.

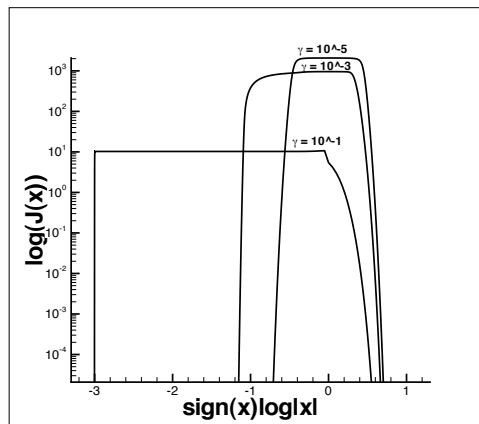


Fig. 4. Solutions of $J(x, \tau)$ of eq.(9) at $\tau = 10^4$. $\gamma = 10^{-1}$, 10^{-3} and 10^{-5} .

We see from Figure 3 that the smaller the parameter γ , the longer the time τ needed to reach the third phase. The red side ($x < 0$) boundary of the profile is very sharp in the third phase. This is because at large $-x$, $\phi(x) \simeq 0$ and $\mathcal{R}(x, x') \simeq 0$, the terms containing $\phi(x)$ and $\mathcal{R}(x, x')$ of eq.(9) can be dropped. Thus, at large $-x$, eq.(9) approximately is

$$\frac{\partial J(x, \tau)}{\partial \tau} \simeq \gamma \frac{\partial J(x, \tau)}{\partial x}. \quad (23)$$

Therefore, the solution generally is $J(\gamma\tau + x)$. The propagation of the sharp “front” will be described by

$$-x \simeq \gamma\tau. \quad (24)$$

Figure 4 presents $J(x, \tau)$ at $\tau = 10^4$, and for $\gamma = 10^{-1}$, 10^{-3} , and 10^{-5} . We can see that the left side boundaries of the profiles roughly satisfy eq.(24).

Figure 5 presents the solutions $J(x, \tau)$ of eq.(9), with the redistribution function given by eq.(5). We take $a = 10^{-3}$. The parameter γ is taken to be 1 and 10^{-1} . We see that the solutions are about the same as their counterparts in Figure 3. The only difference is that $J(x, \tau)$ has long wings in both sides of the central profile. The intensity of the wings is very low. Therefore, $a \neq 0$ does not affect the basic features of the profile of $J(x, \tau)$ at resonant frequency $x \simeq 0$. Its evolution can still be described by the three phases.

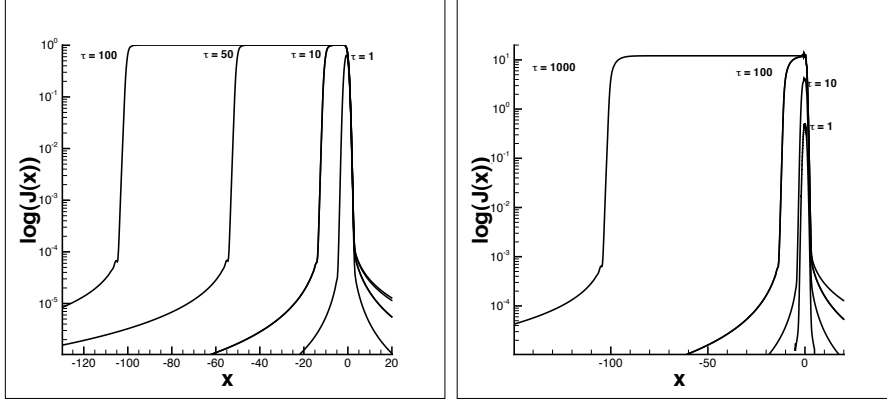


Fig. 5. Solutions of $J(x, \tau)$ of eq.(9) with the redistribution function given by eq.(5). The parameters $a = 10^{-3}$, and $\gamma = 1$ (left) and $\gamma = 10^{-1}$ (right).

6 Time-scale of the W-F coupling

We now estimate the time scale, τ_{WF} , of the onset of the W-F coupling. As mentioned in Section 1, most works on the effect of the W-F coupling of 21 cm signal are based on the static solution of the Fokker-Planck approximation eq.(11) (Chen & Miralda-Escude, 2004; Hirata, 2006; Furlanetto & Pritchard 2006; Chuzhoy & Shapiro 2006). Obviously, this solution corresponds to the third phase of Section 5, in which the central part ($|x| \simeq 0$) of the frequency distribution $J(x, \tau)$ is time independent. Thus, using the static solution of the Fokker-Planck equation is equivalent to assuming that the time scale of the W-F coupling is of the order of τ_{III} . Therefore, this approximation would be reasonable if the time scale of the formation and evolution of the 21 cm signal regions is larger than τ_{III} .

From Figures 3 and 5, one can see that the time scale of the onset of the third phase, τ_{III} , has to be of the order of 10, 10^2 , and 10^4 for $\gamma = 1$, 10^{-1} , and 10^{-3} respectively, i. e. τ_{III} is roughly equal to a few to ten of Gunn-Peterson optical depth. On the other hand, we can see from eq.(10) that $\gamma = 1$, 10^{-1} , and 10^{-3} correspond to $f_{HI} = 10^{-5}$, 10^{-4} , and 10^{-2} for the source at redshift $1+z = 10$. Thus, for all cases, eq.(7) yields that the time scale t_{III} to be of the order of 1 Myr. Therefore, the static solution of the Fokker-Planck equation would not be valuable for the 21 cm problem, if the time scale of the evolution of the 21 cm region is equal to or less than 1 Myr.

Actually the time-independent solution of eq. (11) is not necessary for the 21 cm signal. The relative occupation of the two hyperfine-structure components of hydrogen ground state depends only upon the shape of the spectrum near the Ly-alpha frequency. What we need for the W-F coupling is only the frequency distribution to be a Boltzmann-like distribution $J(x, \tau) \propto \exp[-h(\nu - \nu_0)/kT]$ around ν_0 , where T is the kinetic temperature of hydro-

gen gas. The formation of the Boltzmann-like distribution is irrelevant to the time scale τ_{III} , but depends on the onset of the second phase of the $J(x, \tau)$ evolution.

However, neither Figure 3 nor Figure 5 shows a Boltzmann-like profile. This is because the recoil of atoms during the scattering has not been considered in eq.(9), which is equal to the kinetic temperature of hydrogen gas to be infinity. Considering the recoil of atoms, the redistribution function for the Doppler broadening is (Field, 1959, Basko, 1981)

$$\mathcal{R}(x, x') = \frac{1}{2} e^{2bx+b^2} \text{erfc}[\max(|x+b|, |x'+b|)], \quad (25)$$

where $b = h\nu_0/mv_Tc = 2.5 \times 10^{-4}(10^4/T)^{1/2}$.

In this paper, we will not re-solve eq.(9) with the redistribution function eq.(25), but use a simple way to estimate τ_{WF} . Field (1959) showed that, once the solution $J(x, \tau)$ of eq.(9) with $b = 0$ (no recoil) has a flat plateau in the central region, the effect of recoil is to make the flat plateau to be a Boltzmann-like distribution, i.e. if the solution with no recoil redistribution eq.(6) shows $J(x, \tau) \simeq J(0, \tau)$, within $|x| < x_f$, the solution of eq.(9) with redistribution eq.(25) will be

$$J(0, \tau) e^{-2bx} = J(0, \tau) e^{-h(\nu-\nu_0)/kT_k}, \quad |x| < x_f. \quad (26)$$

Therefore, τ_{WF} should be estimated by the time scale of the onset of the second phase, τ_{II} , not by τ_{III} . For small γ , τ_{II} is much less than τ_{III} . For instance, τ_{III} will be as large as $\tau \simeq 10^6$ for $\gamma = 10^{-5}$, while Figure 6 shows that a small flat plateau has already formed at $\tau = 10$.

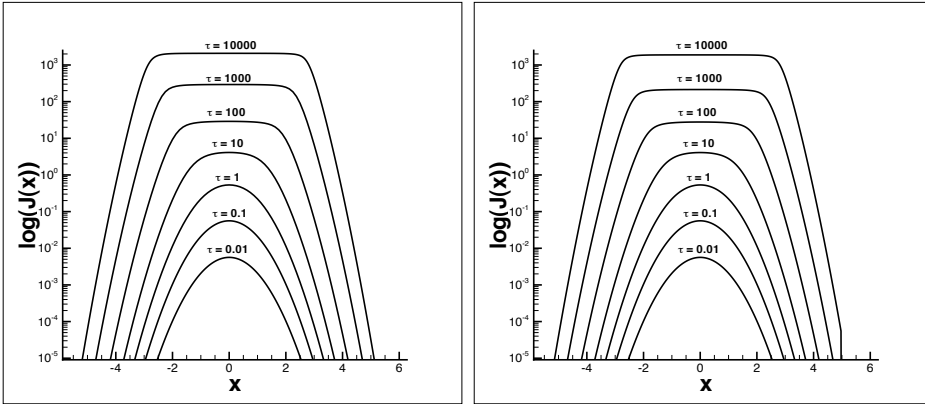


Fig. 6. Solutions of $J(x, \tau)$ of eq.(9) with parameters $a = 0.$ and $\gamma = 10^{-5}$ (left panel) and 10^{-7} (right panel).

The flatness of the flat plateau in a range $|x| < x_f \equiv (\nu_f - \nu_0)/\Delta v_D$ can be

measured by

$$F(\tau) = \frac{\ln J(x_f, \tau) - \ln J(0, \tau)}{x_f}. \quad (27)$$

The frequency width of the flat plateau, $|\nu_f - \nu_0|$ should be equal to or larger than the frequency of the 21 cm photon, that is $|\nu_f - \nu_0| \geq \nu_{21} = 1420$ MHz. We have then

$$x_f \geq 0.014 \left(\frac{10^4}{T} \right)^{1/2}. \quad (28)$$

In order for the flat plateau to show a Boltzmann distribution $J(0, \tau)e^{-2bx}$ [eq.(26)], the flatness $F(\tau)$ within x_f should be given by $F(\tau) \ll b$. Therefore, the time scale τ_{WF} can be estimated by the solution of the following equation

$$F(\tau) = b = 2.5 \times 10^{-4} (10^4/T)^{1/2} \simeq 0.018x_f. \quad (29)$$

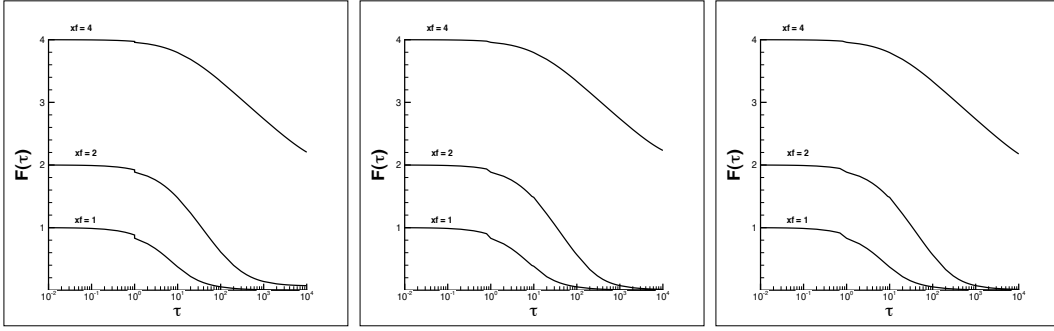


Fig. 7. $F(\tau)$ as function of τ for solutions of $a = 0$ and $\gamma = 10^{-3}$ (left), 10^{-5} (middle) and 10^{-7} (right). x_f is taken to be 1, 2 and 4.

In Figure 7, we show the function $F(\tau)$ for the parameters $(a = 0, \gamma = 10^{-3})$, $(a = 0, \gamma = 10^{-5})$, and $(a = 0, \gamma = 10^{-7})$. It is interesting to observe that the three sets of $F(\tau)$ shown in the three panels of Figure 7 are almost identical. That is, the time scale τ_{WF} is actually independent of the parameter γ . For all the three cases of the parameter γ , τ_{WF} is equal to about 10^2 for $x_f = 1$, and 10^3 for $x_f = 2$. In other words, a flat plateau with proper width can form with a few tens or few hundreds of the mean free flight time of the resonant photons, regardless the expansion of the universe.

The reason of the γ -independence of τ_{II} and τ_{WF} can be directly seen from eq.(9). This equation describes two kinetic processes of approaching statistically steady state described. The first is the resonant scattering, which leads to the formation of a uniform distribution in frequency space, i.e. a flat plateau, around the resonant frequency. The second is the redshift of photons, which

leads to a statistical equilibrium between the injected photons and redshifted photons. The steady state due to resonant scattering corresponds to the second phase, while the steady state due to redshift corresponds to the third phase. Similar to various statistical equilibrium or steady state maintained by collision or scattering, the steady state of resonant scattering can be realized via a few or few tens of the resonant scattering. On the other hand, γ is a ratio between the time scales of the resonant scattering and the expansion of the universe. Therefore, when γ is much less than 1, the time scale of the formation of the flat plateau is independent of γ . This point can also be seen with Figure 6, which shows that for $\gamma = 10^{-5}$ and 10^{-7} the evolutions of $J(x, \tau)$ actually are the same till $\tau = 10^4$. In short, the W-F coupling will take place once a statistical equilibrium localized around the resonant frequency is realized.

7 Concluding remarks

To study the time scale of the W-F coupling, we need a better solution of the integro-differential equation of the resonant scattering of Ly α photons. Especially, we need to know the formation and evolution of the flat plateau of the photon frequency distribution around the resonant scattering. That is, the algorithm should be able to handle the extremely flat distribution and its sharp boundary. These features can properly be captured by the WENO scheme, which has high order of accuracy and good convergence in capturing discontinuities as well as to be significantly superior over piecewise smooth solutions containing discontinuities. We show that the WENO solutions can precisely match the analytic solutions of the evolution of photon distribution function in rest background.

We solve the equations of resonant scattering without recoil with constant source in the expanding universe. The evolution of the photon distribution in the frequency space generally undergoes three phases. In the first phase, the profile of the photon distribution is similar to the initial one. In the second phase, an extremely flat plateau forms around the resonant frequency, and the width and height of the flat plateau increase with time. Finally, in the third phase, the photons injected from the source is balanced by the redshift of the expansion, and the evolution of the photon distribution is stable. The first phase is very short. The second phase will be onset after a few scattering of photons by atoms. On the other hand, the onset of the third phase is mainly dependent on the Gunn-Peterson optical depth, which is large at early universe. Consequently, the onset of the third phase is much later than the second one.

Usually, the W-F coupling is described by time-independent solutions of the

Fokker-Planck approximation of the integro-differential equation of the resonant scattering. With the WENO solutions, we show that the time-independent solutions would not be available for the 21 cm signal of the first generation stars, if the life time of the evolution of the 21 cm region is equal to or less than 1 Myr. However, the time scale of the onset of the W-F coupling actually is irrelevant with the time-independent solutions. The W-F coupling will take place once a statistical equilibrium is locally realized in the frequency space around the resonant frequency. This time scale is always a few tens or hundreds of the mean free flight time of the resonant photons, and is generally independent of the expansion of the universe when the Gunn-Peterson optical depth is large, or the Sobolev parameter is much less than 1.

Acknowledgments

This work is supported by the US NSF under the grants AST-0506734 and AST-0507340. We thank Dr. Jiren Liu for his help.

References

- [1] Basko, M.M. 1981, *Astrophysics*, 17, 69
- [2] Carrillo, J.A., Gamba, I.M., Majorana, A. & Shu, C.-W. 2003, *J. Comput. Phys.*, 184, 498
- [3] Carrillo, J.A., Gamba, I.M., Majorana, A. & Shu, C.-W. 2006, *J. Comput. Phys.*, 214, 55
- [4] Cen, R. 2006, *ApJ*, 648, 47
- [5] Chen, X. & Miralda-Escude, J. 2004, *ApJ*, 602, 1.
- [6] Chuzhoy, L., Alvarez, M. A., & Shapiro, P. R. 2006, *ApJ*, 648, L1
- [7] Chuzhoy, L. & Shapiro, P.R. 2006, *ApJ*, 655, 843
- [8] Field, G.B., 1958, *Proc. IRE*, 46, 240
- [9] Field, G.B. 1959, *ApJ*, 129, 551.
- [10] Furlanetto, S.R. & Pritchard, J.R. 2006, *MNRAS*, 372, 1093
- [11] Henyey, L.G. 1941, *Proc. Nat. Acad. Sci.* 26, 50
- [12] Hirata, C.M. 2006, *MNRAS*, 367, 259
- [13] Hummer, D.G. 1962, *MNRAS*, 130, 295
- [14] Hummer, D.G. 1969, *MNRAS*, 145, 95
- [15] Hummer, D.G. & Rybicki, G.B. 1992, *ApJ*, 387, 248.
- [16] Jiang, G. & Shu, C.W. 1996, *J. Comput. Phys.*, 126, 202
- [17] Liu, J.R., Qiu, J.M., Feng, L.L., Shu, C.W. and Fang, L.Z. 2007, *ApJ*, 663, 1
- [18] Meiksin, A. 2006, *MNRAS*, 370, 2025
- [19] Qiu, J.M., Feng, L.L., Shu, C.W. & Fang, L.Z. 2006, *New Astronomy*, 12, 1
- [20] Qiu, J.M., Feng, L.L., Shu, C.W. & Fang, L.Z. 2007, *New Astronomy*, 12, 398

- [21] Qiu, J.M., Shu, C.W., Liu, J.R. & Fang, L.Z. 2008, *New Astronomy*, 13, 1
- [22] Rybicki G.B. & Dell'Antonio, I.P. 1994, *ApJ*, 427, 603
- [23] Shen, J., Shu, C.W. & Zhang, M. 2007, *J. Sci Comput*, 33, 279
- [24] Shu, C.-W., 2003, *Int. J. Comp. Fluid Dyn.*, 17, 107
- [25] Shu, C.-W. & Osher, S., 1988, *J. Comp. Phys.*, 77, 439
- [26] Wouthuysen, S. A. 1952, *AJ*, 57, 31